SLAC – PUB – 3760
August 1985
(A)

Properties of Thin Anti-Multipactor Coatings for Klystron Windows*

A.R. NYAIESH, E.L. GARWIN, F.K. KING AND R.E. KIRBY

Stanford Linear Accelerator Center
Stanford University, Stanford, California, 94305

ABSTRACT

Low secondary electron emission yield (1-1.3), low rf-loss films are of interest as coatings for alumina ceramic high power klystron windows. Very thin (15-50Å) Ti and TiN layers have been previously used with success in klystron tubes operating at lower power levels (<35 MW peak power) and short (2.5 μsec) pulses but are subject to property changes during air exposure, tube bakeout (550°C for up to 10 days) and in-situ electron bombardment. Higher power tubes ($\geq$50 MW) with longer (5 μsec) pulse lengths require coatings that remain stable under these more rigorous conditions in order to avoid multipactoring and window failure due to overheating.

Air-oxidized Cr films offer an alternative to TiN. This work shows that they have the required resistivity for low rf-loss, combined with stability in the secondary electron emission (SEE) yield under bakeout and electron bombardment.

* Work supported by the Department of Energy, contract DE – AC03 – 76SF00515.

Presented at the 32nd National Symposium of the American Vacuum Society, Houston, Texas, November 19-22 1985.

SEE, AES, XPS, ELS, oxidation, bakeout and electron bombardment results are presented for Cr and TiN layers deposited by sputtering onto high density alumina substrates. The surface of TiN oxidized to a 9Å thick TiO_2 layer which, under bakeout to 550°C in vacuum, thinned to 6Å. This extreme layer-thinness resulted in a significant drop in the SEE yield which, unfortunately, was reversible upon re-oxidation. The oxidized layer on Cr was 17Å of Cr_2O_3 which thinned to 13Å upon bakeout. This thicker oxide layer produced a stable SEE yield which, although not as low as oxidized TiN, is sufficient to prevent electron multipactor.

Windows covered by air-oxidized Cr films are at least as good, under tube processing conditions, as the best TiN-coated windows.

1. Introduction

High-power klystron tube manufacture is subject to a wide variety of difficulties related to incoming material control, polishing and cleaning of components, contamination during assembly and testing and, in addition, processing and operational failures. Of particular interest to this paper are failures which occur to the tube's alumina (Al_2O_3) ceramic output window.

Two of the most common problems in use are: 1) alumina window breakage due to overheating and breakdown caused by electron multipactor (resonant multiplication of electrons generated at the high secondary electron yield alumina surface) and, 2) overheating due to excessive rf losses in the coating applied to the ceramic to control multipactor. For lower power levels (<35MW peak power) and short (2.5 μsec) pulses these two problems have been adequately controlled by coating the alumina with a thin (15-50Å) high resistivity (100 MΩ/square) low total secondary electron yield ($\sigma < 1.5$) $TiN_{x\cong 1}$ layer. However, higher power tubes ($\geq$ 50 MW) with longer pulse lengths (5 μsec) require extremely close control over the deposition conditions and areal density of such a layer, as well as special handling and baking provisions.

Superconducting rf cavities for storage rings also suffer from multipactor. At SLAC, an extensive surface physics program is in progress for determining the suitability of various materials (particularly metalloids, such as TiN) for use as anti-multipactor coatings[1]. Some of these studies are applicable to the klystron window problem as well. Briefly, our results show that clean low-Z metals and metalloids have low total secondary electron yields (σ), typically 0.9 to 1.2. These yields rise significantly upon air exposure (which results in oxidation and airborne hydrocarbon and water contamination) to values usually greater than 1.5. Electron bombardment of the coating (as occurs during tube processing) causes some reduction of the yield but not to the as-deposited level.

In the past, processing of a cleaned window for a tube proceeded as follows: The window was coated on both sides by plasma sputtering of 15-50Å of TiN.

It was removed from vacuum, mounted on a tube, which was then evacuated, and baked for up to 10 days at 550°C with the output side of the window also evacuated. The cathode was activated, and then the output side of the window was exposed to air. Results presented in this paper show that the yield of TiN-coated windows can be very different on the tube and load sides, particularly when the tube is subsequently operated under increasing power levels ("conditioning") which may still further reduce the yield on the tube side. As a result of our surface studies, standard practice is now to pre-bake TiN-coated windows for $\sim$ 24h at 550°C, and then expose to air, thus stabilizing the coating against these effects.

We show that, for air-oxidized Cr films, the yield is more stable under simulated tube processing conditions than for TiN films and, in addition, Cr-coated windows are capable of withstanding operation at 100 Mwatt of rf power, 6 μsec pulse length, without thermal- or multipactor- induced failure. These windows are at least as good as the best TiN-coated windows.

2. Experiment

2.1 Surface Analysis System

Samples were analyzed in an ion-pumped, baked ultrahigh vacuum system ($P<3x10^{-10}$ Torr) incorporating XPS, AES, ELS, and total secondary electron emission yield (σ) techniques. Measurements utilized very low probe currents and counting techniques to minimize electron damage to the oxides. No such damage was observed.

Measurements of the secondary electron yield, σ, were done via the retarding potential difference method[2] at 2 nA primary electron current. The AES electron beam was 50 nA, rastered to give a current density of 2×10^{-3} A/m^2. Binding energy references for XPS are the Pd Fermi edge (BE=0) and the Ag $3d_{5/2}$ core line (BE = 368.2 eV). The x-ray anode used was Mg K$\alpha_{1,2}$ (hν=1253.6

eV) at 240 watts anode input power. The electron energy analyzer imaged a 4 x 4 mm^2 area of the sample during analysis. Close monitoring of binding energy references and power supply linearity assure that the binding energy values presented here are accurate to $\pm$ 0.1eV.

2.2 Sample Preparation

The substrates used were 1 cm diameter x 0.06 cm thick discs of 99.5%-pure alumina. The substrates are mounted in a 1.6 cm diameter x 0.5 cm thick Nb carrier for transfer (*in vacuo*) to the sample carousel. The 140Å thick TiN films were produced by sputtering onto ambient temperature substrates using a Kaufmann ion source bombarding a 99.9%-pure compacted powder TiN target with an Ar pressure of 7 x 10^{-5} Torr and a deposition rate of 0.3 Å/sec at 1500eV ion energy. The 140Å Cr films were produced by magnetron sputtering from an electrodeposited 99.99%-pure Cr target. The operating conditions were: 5 x 10^{-3} Torr Ar at 0.2A discharge current, 300 V applied voltage, 0.1 m target-substrate separation and a deposition rate of 3.5Å/sec.

A thickness of 140Å was chosen because this is sufficiently thick to prevent substrate backscatter from contributing to the secondary yield measurements, while appearing as a bulk layer for XPS and AES measurements. Since the layers did not oxidize through, they were also effective in preventing charging during measurement.

Samples were oxidized by exposure to room air at 24°C, 50% R.H. Electron bombardment of the layers was done using a scanning electron gun at 500eV and 100nA beam current covering 1 cm^2 at the sample. The sample during bombardment was biased at +70 V relative to the chamber, producing an effective electron energy of 570 eV and a current density of 1 x 10^{-3} A/M^2.

3. Results

To simulate the sequence of events which occurs in tube processing, the Cr and TiN films are sputtered onto clean substrates, exposed to air for approximately 12 hours and inserted into the surface analysis chamber. They were heated for 10 hours at 550°C although we have found that 2 hours are sufficient to substantially complete any thermally induced changes that occur. The sample is analyzed for σ, AES and XPS; in that order because σ is most sensitive to surface condition. The sample is transferred to a load lock and exposed to room air for 1 hour, pumped, and reanalyzed. To investigate the effects of conditioning, the sample is bombarded by 3 x 10^{17} electron/cm^2 and again re-analyzed.

Figures 1-4 show the results of this sequence for σ and the XPS 2p core levels of Cr and Ti. The improved stability of Cr over TiN is quite apparent in the SEE yield. The source of this stability is discussed further in this paper. Rf tests show that σ for Cr, although not as low as that for TiN, is adequate to prevent multipactor. The AES results for TiN/alumina indicate some oxygen gain/loss during these various cycles (shown by the XPS results also), however, the Ti and N AES lines overlap, making them difficult to interpret compared to the XPS Ti and N core lines. Therefore, we have concentrated on presenting the XPS results, particularly their chemical aspects and only present AES results where they supplement the XPS.

The improved thermal stability of Cr oxide over TiN is readily apparent in Figures 5 and 6 which show that σ for Cr is unaffected by bake temperature or time, once surface gases have desorbed. It should be emphasized that in addition to thermal stability and low σ, these window films must have a high enough surface resistance (100 mΩ/square) to limit rf losses at the window surface. As mentioned in the Introduction, the first tests of Cr-coated windows under processing/operating conditions have been successful. In addition, no evidence of multipactor was observed in the tubes.

4. Discussion

It is useful to determine the changes in chemical states which lead to the stability in the Cr layer and relative lack of it in the TiN layer. Accordingly, we have curve-fitted the core level spectra in both the oxidized and oxidized/heated configurations for each type of layer.

Briefly, the curve fitting procedure is as follows. Each core level is doubled by the spin-orbit splitting with a well-defined energy separation and intensity ratio between the peaks. The experimental spectra of Figures 7, 9, 12 and 14 will contain at least four peaks, oxide and metal for Cr and oxide and nitride for TiN. From other XPS core level measurements we have made, the position, separation and intensity ratios for clean Ti, TiN, TiO_2, Cr and Cr_2O_3 spin-orbit-split peaks are known. These clean spectra are used for starting conditions to fit the experimental data. The theoretical peaks for the fit have a Doniach-Sunjic lineshape[3] characterized by parameters such as halfwidth, energy position, asymmetry, phonon broadening and background, all of which may be entered as variables. The theoretical lineshapes are convolved with the Mg x-ray lineshape and electron energy analyzer transmission function. The computer program doing the fit is constrained to move by fitting peaks in pairs in order to reflect the spin-orbit splitting constraint. The program uses an analytical solution to a linearized fitting function with a gradient search in N-dimensional parameter space to find the lineshape values which give the smallest value reduced chi-squared (χ^2) fit to the raw data. A perfect fit would have a reduced χ^2 of one but very good fits are characterized by reduced χ^2 of less than two.

The critical steps in tube processing are the air exposure and bakeout. Using curve fitting, we examine the chemistry that occurs on our model surfaces for both TiN-and Cr-coated alumina. First we consider the TiN layer. Figure 7 is the Ti 2p core spectrum for a 140Å TiN layer (on Al_2O_3) which has been exposed to air overnight, (although this spectrum is not significantly different from a 1 hour air exposure). Figure 9 is a Ti 2p spectrum for that surface heated to 550°C

for 10 hours and allowed to cool to room temperature prior to taking the spectra. Figures 8 and 10 are the O 1s and N 1s core levels corresponding to Figures 7 and 9.

The sequence of events which occurs, as will be shown, is the following: The TiN, upon air exposure, oxidizes to 2-3 monolayers of TiO_2. There is evidence for the existence of sub-oxides of Ti, particularly TiO, presumably all located between the TiO_2 and TiN. The N freed as a result of oxidation apparently remains below the TiO_2 layer, possibly interstitially or in the grain boundaries. Additionally, there is some H_2, CH_4, CO, CO_2 and water (OH^-) adsorbed on the surface.

During heating to 550°C the adsorbed gases desorb and some of the TiO_2 dissociates and is converted to TiN, or possibly Ti-oxynitride, by combination with the trapped N. The thinning of the TiO_2 layer and the gas desorption results in a sharp drop in the secondary electron yield. The entire sequence of events can be repeated if this surface is again re-exposed to air.

When Cr layers on alumina are exposed to air and heated in the same manner as TiN layers, the results are rather simpler. The Cr-oxide formed is 8 monolayers thick and reduces to 6 monolayers during heating. H_2 is desorbed with little else. Subsequent air exposure leaves the surface essentially unchanged.

In order to identify the various curve fit components, we have measured reference XPS spectra for air-oxidized Ti(TiO_2) and Al(Al_2O_3), clean Ti and TiN, and clean Cr and Cr_2O_3. Where necessary, these reference spectra have been curve fit using the above-described procedure, the binding energies and peak areas determined and the results for the standards compared to the literature for confirmation. Table I presents the results for these reference peaks, giving the binding energy positions, areal ratios and literature references where available.

Oxidized TiN on Al_2O_3

Examination of the Ti 2p spectra of Figure 7 shows the readily-identifiable presence of TiO_2 and TiN. There is also the possible presence of Ti-sub oxides

at ~457 eV which might also be Ti-oxynitride[9]. If present, TiO occupies the same energy position as TiN[4]. The largest peaks in the O 1s and N 1s spectra of Figures 8 and 10 are due to oxides and nitride of Ti. Except for the possible presence of O 1s from chemisorbed oxygen or OH^-[11], no other peaks of oxygen or carbon for adsorbed gases were observed in XPS and less than 1% of a monolayer of C observed in AES.

Since only one peak is likely present at the TiO_2 position, the analysis starts at that point. The Ti peaks 3 of Figure 7 are due to TiO_2 and therefore, using the reference TiO_2 areal ratio of Table I, we can calculate the oxygen peak area that should appear at the oxide position (peak 2, Figure 8). That calculated area is smaller than that which is actually measured, i.e. other oxide(s) in addition to TiO_2, are present. Assuming that the same XPS atomic sensitivity can be used for both TiO_2 and its other oxides, the excess oxygen could be assigned to TiO and, say, Ti_2O_3. Similarly, the N 1s peak at 397.4 eV of Figure 8 is due most likely to TiN. Using the reference areal ratio for TiN shows an excess of Ti peak area at the 455.2 eV position of Figure 7. If the excess Ti is assumed to be combined as TiO with part of the excess oxygen such that this new Ti/O ratio is 2 times the Ti/O ratio for TiO_2 (i.e. 2.12) then any remaining excess O may be combined with the Ti core peak at 457.1 eV to determine the likely Ti-sub oxide stoichiometry. In fact, that final quantity turns out to be Ti/O = 1.59, i.e., close to Ti_2O_3 whose Ti/O areal ratio (compared to TiO_2 at 1.06) would be 1.42.

The presence of Ti-oxynitride as the source of the Ti core peak at 457.1 eV seems unlikely because a N 1s peak at around 398.4 eV would also arise[9] and none is observed here. Using the areas measured here for the TiO_2 reference and the TiO_2 + TiN overlayer, a calculation of the TiO_2 overlayer thickness yields 8.8Å or about three monolayers. Dry O_2 oxidation of TiN at 550°C has been shown to result in the formation of rutile TiO_2[12]. Table II presents the energies and areas measured for the various peaks used in the analyses for both the oxidized and the oxidized and heated TiN surfaces.

Focussing attention on the O 1s and N 1s spectra of Figure 8, we find the major O 1s peak at 530.5 eV which is characteristic of Ti-oxide and was used to make the above analyses. The smaller peak at 532.2 eV is due to the alumina substrate (in addition to chemisorbed oxygen) for the simple reason that there is a very small Al 2p peak detectable as well. Using the reference Al/O areal ratio for Al_2O_3 covered by a 140Å TiN + TiO_2 overlayer, the Al/O ratio for O at 532.2 eV should be ~1.25. The measured ratio is 0.5 for the oxidized surface and 0.37 for the oxidized and heated surface. That indicates that there is O 1s intensity present due to chemisorbed oxygen and/or water (hydroxyls).

The N 1s spectrum of Figure 8 has two peaks, one of which is clearly TiN and the other of which could be assigned to chemisorbed N[11], interstitial N, or possibly N in the grain boundaries. Adsorbed N seems unlikely because 1) surface N would likely be replaced by hydroxyls and hydrocarbons during the air exposure and, 2) if present on the surface in other forms, e.g. NO, would produce a peak at higher binding energy than that observed[11]. Interstitial N or possibly N trapped in grain boundaries is appealing in view of a model of growth of TiO_2 which moves inward into the TiN film and traps the N released by oxidation of TiN, at least at room temperature. Also, the very long asymmetric kinetic energy loss tail on the 396.4 eV N 1s peak suggests a sub-surface origin for this component, just as a similar loss tail is seen in the Ti-sub-oxide peak of Figure 7.

Oxidized and Heated TiN on Al_2O_3

The oxidized TiN on Al_2O_3 was positioned near the entrance of a quadrupole mass spectrometer and heated radiantly from the rear by a W pancake filament. The gases observed desorbing from the sample and holder were H_2(40%), CO(24%), Ar(23%), H_2O(6%), CH_4(4%) and CO_2(3%). The Ar was probably incorporated into the TiN during deposition. The coverage on the sample prior to heating was low for carbon-containing molecules, as pointed out previously.

Figures 9 and 10 and Table II show: 1) a drop in the Ti core for TiO_2, 2) a

rise in the Ti core for TiN + TiO, 3) an 0.5 eV shift to higher binding energy for O 1s from oxide, 4) a transfer of N 1s intensity from the interstitial state into the nitride state; 5) a rise in the total N 1s peak area, 6) a small drop in the O 1s oxide peak area and, 7) a small increase in the Ti peak area at 457.0 eV as well as a broadening of that peak. Again, no extra peak is observed to appear in the N 1s core level which might indicate the presence of oxynitrides. Attempting to carry out an an areal ratio analysis like that for the oxidized surface, the following is determined. Assuming again that all the Ti intensity at 458.9eV is due to TiO_2, the thickness of the TiO_2 layer drops from 8.8Å to 6.3Å. If this is the case, a significant decrease in the oxygen peak in both the XPS ($\lambda = 19.7$Å) or the AES ($\lambda = 16.6$Å) is expected. A rather smaller reduction of 7% is seen in the total O 1s peak at 530.5 eV (now shifted to 531.0eV) and almost no reduction in the AES O peak. This suggests that most of the O freed from TiO_2 remains in the surface region and may be there as suboxides and chemisorbed O or OH^- since the peak at 532.2 eV does grow as a result of heating. The discussion above about the source of the O 1s peak at 532.2 eV indicated that it was partly due to the alumina substrate. No change is observed in the Al 2p intensity after heating and, therefore, the increase seen in O at 532.2 eV must be due to chemisorbed O or OH^-.

Although the bulk melting point of TiO_2 is 1850°C, there is evidence in the literature[13] for TiO_2 on Ti layers which indicate that TiO_2 decomposes at 400°C or so. The 0.5 eV shift to higher binding energy in the O 1s (oxide) and 0.2 eV shift in the Ti (TiO_2) suggests that the as-oxidized TiO_2 layer was actually somewhat oxygen-deficient and the heating breakdown of the TiO_2 provided adequate oxygen to make the remaining layer stoichiometric TiO_2.

Using the Ti/N areal ratio (4.21) of our reference TiN and the N 1s intensity at 397.3 eV for the heated surface indicates that there is insufficient Ti intensity at 455.2 eV in Figure 9 to maintain this ratio, i.e., there is "too much" N. Since there is a drop in the adsorbed/interstitial N peak at 396.3 eV, the suggestion might be that the stoichiometry of the TiN after heating is different from that

before. However, a change in TiN stoichiometry to higher N content should result in an increase in the binding energy difference between the Ti 2p and N 1s peaks due to an increase in charge transfer[14]. That is not observed here as both Ti and N peaks preserve their energy positions. Part of the intensity increase in the Ti (nitride) peak and the N (nitride) peak after heating is due to a thinning of the absorbing TiO_2 overlayer. If that thinning is taken into account, the total N 1s signal is essentially unchanged by the heating. What does appear to occur, however, is a transfer of 70% of the intensity from the adsorbed/interstitial N peak into the nitride peak located at 397.4 eV. Since that extra "TiN" N 1s intensity is not assignable to TiN, another source must be postulated. There is some broadening of the Ti-suboxide peak, so perhaps a weak oxynitride is appearing. Another possibility might be the formation of NH or something similar on the surface. Figure 11 is a series of reflection ELS spectra for the various reference surfaces as well as the oxidized and oxidized/heated TiN on Al_2O_3 surfaces. Of particular interest is feature number 4 of curve (e) which appears to be a TiN-like structure but occurs at too low a loss energy. A 50-50% synthesis of TiO_2 and TiN (curve f) matches the rest of the curve (e) nicely, however. So feature 4 of curve (e) may represent a graded composition between the TiO_2 and TiN. In such a case, it might be appropriate to assign some portion of the Ti-suboxide intensity of Figure 9 and some of the N to a weak oxynitride.

The analysis of the oxidized and oxidized/heated TiN on Al_2O_3 surfaces as presented above is sufficient to determine why the secondary electron yield (σ) drops after heating. Some of the drop is due to gas desorption but a portion of the drop can be attributed to the reduction of the TiO_2 layer thickness from 8.8Å to 6.3Å. Work on SiO_2 on Si surfaces[15] shows that the yield drops sharply as the oxide overlayer thickness decreases. The effect appears smaller for SiO_2 on Si than for our TiO_2 on TiN layer but σ for the clean Si surface could not be measured[15] and, therefore, the initial increase in σ upon oxidation may be more rapid than can be inferred from the more heavily oxidized Si results. Also, the absolute value of σ for Si was not measured but rather the σ ratio for different

Si-oxide layer thicknesses, making a direct comparison of our results to the Si results impossible.

Oxidized Cr on Al_2O_3

Figures 12-14 and Table III present the results for Cr/alumina. Examination by AES and XPS of the oxidized surface showed 5-10% of a monolayer of C present which mostly is removed during the first heating of the surface. The mass desorption spectrum showed 87% H_2, 5% H_2O, 4% CO, 2% CO_2 and 1.5% CH_4 leaving the sample and holder. The H_2 was presumably gettered by the fresh Cr film during deposition and was possibly present in the stainless sample holder.

The sequence of events involved in the oxidation and heating of the Cr layer appear straightforward. The as-deposited film (Figures 12 and 13) oxidizes to Cr_2O_3. This is supported by the binding energy position of the Cr $2p_{3/2}$ core line and by the Cr(576.9 eV)/O areal ratio, both of which agree with our Cr_2O_3 reference. The energy Cr 2p position of 576.9 eV is essentially identical to our Cr_2O_3 reference although little difference in binding energy for $Cr^{3+}(Cr_2O_3)$ and $Cr^{4+}(CrO_2)$ states has been observed[16,17]. More to the point, CrO_2 is typically produced under excess O conditions and is converted to $Cr^{6+}(H_2CrO_4)$ by exposure to H_2O[16]. Cr^{6+} would be easily detectable[17] in our Cr spectra. The Cr/O areal ratio of our references is 1.54, the oxidized Cr layer, 1.56 and the heated layer, 1.46. A ratio of 1.28 would be expected for CrO_2 from atomic ratio considerations. Numerous studies show that oxidation of Cr in O_2 or air leads to the formation of Cr_2O_3[18–20].

A calculation of the Cr_2O_3 layer thickness after oxidation yields 17.1Å. A thickness of ~10Å has been inferred from O_2 and air-oxidation by photoemission[19] and STEM[20]. The underlying (if indeed, it is "underlying") Cr metal signal is about half that calculated for a uniform 17.1Å Cr_2O_3 overlayer. Strong defect scattering in the Cr_2O_3 overlayer could reduce the Cr metal signal, a situation that could be expected on a rough alumina surface. The rather thick (8 mono-

layers) Cr_2O_3 would be expected to also have a lower yield than that usually expected for insulators if it has a high concentration of defects.

Oxidized and Heated Cr on Al_2O_3

Heating the oxidized Cr layer on alumina results in a) a drop in the Cr_2O_3 thickness, b) an increase in the Cr metal signal c) a small drop in the O signal and d) a drop in the Cr/O ratio from 1.56 to 1.46. The results are presented in Table III. The new Cr_2O_3 thickness is 13.3Å and, again, the Cr metal underlayer signal is smaller than expected for a uniform layer picture, although the discrepancy is smaller (60% of that expected) than that of the oxidized-only case. This improvement in the underlayer signal may be due to the annealing out of defects and general improvement in the Cr_2O_3 film quality. Indeed, there is a reduction in the secondary electron background in the XPS spectra following the heating cycle (compare Figures 12 and 14 and see Figure 13).

Since there is no change in the binding energies of the Cr and O core lines, no further chemistry takes place during heating but the re-arrangement occuring is responsible for the drop in Cr(576.9eV)/O areal ratio. Indeed, the total Cr(metal plus oxide) signal is unchanged by the heating. It is possible that the slight drop in O signal may be due to desorption of chemisorbed O or OH^- but the binding energy for such a species would have to coincide with that for the oxide.

5. Conclusion

The results for TiN on alumina show that the large changes seen in σ for this layer is due to thinness of the TiO_2 layer formed during air exposure. This TiO_2 is subject to decomposition on heating and, since the secondary emission coefficient is very different for TiN and TiO_2, the result is a widely varying σ under typical klystron processing conditions.

The corrosion layer covering on Cr on alumina is considerably thicker and relatively stable under heating. The apparently high defect concentration in the

Cr_2O_3 layer is responsible for the relatively low secondary yield (compared to other insulators) of the coated windows.

6. References

1. I.E. Campisi, H. Deruyter, Z.D. Farkas, E.L. Garwin, H.A. Hogg, F. King and R.E. Kirby, IEEE Trans., Nucl., Sci. NS-30, 3363(1983).
2. V.E. Henrich, Rev. Sci. Instrum. 45, 861(1974).
3. S. Doniach and M. Sunjic, J. Phys. C 3, 285(1970).
4. L. Porte, M. Demosthenous and Tran Minh Duc, J. Less Common Met. 56, 183(1977).
5. M. Textor and R. Grauer, Corrosion Sci. 23, 41(1983).
6. H. Höchst, R.D. Bringans, P. Steiner and Th. Wolf, Phys. Rev. B 25, 7183(1982).
7. J.A. Leiro and E.E. Minni, Phil. Mag. B 49, L61(1984).
8. I. Ikemoto, K. Ishii, S. Kinoshita, H. Kuroda, M.A. Alario Franco and J.M. Thomas, J. Sol. State Chem. 17, 425(1976).
9. K.S. Robinson and P.M.A. Sherwood, Surf. and Inter. Anal. 6, 261(1984).
10. M.P. Seah and W.A. Dench, Surf. and Inter. Anal. 1, 2(1979).
11. M.W. Roberts, in Advances in Catalysis, Vol. 29, Academic Press, New York, (1980).
12. M. Wittmer, J. Noser and H. Melchior, J. Appl. Phys. 52, 6659(1981).
13. E. Bertel, R. Stockbauer and T.E. Madey, Surf. Sci. 141, 355(1984).
14. L. Porte, L. Roux and J. Hanus, Phys. Rev. B 28, 3214(1983).
15. K. Okamoto, Rev. Sci. Instrum. 51, 302(1980).
16. F. Garbassi, E. Mello Ceresa, G. Basile and G.C. Boero, Applic. Surf. Sci., 14, 330(1983).
17. C.N.R. Rao, D.D. Sarma, S. Vasudevan and M.S. Hedge, Proc. R. Soc. Lond. A 367, 239(1979).

18. J.C. Fuggle, L.M. Watson, D.J. Fabian and A. Affrossman, Surf. Sci. 49, 61(1975).

19. G. Gewinner, J.C. Pruchetti, A. Jaegle and A. Kalt, Surf. Sci. 78, 439(1978).

20. F. Watari, Surf. Sci. 110, 111(1981).

Table I XPS References

Surface	$2p_{3/2}$	O1s	N 1s	Ti/O	Ti/N	Cr/O	Literature[f]
Ti[a]	454.0	–	–	–	–	–	454.0[4]
Al_2O_3[b]	–	532.5	–	–	–	–	532.4[5]
TiN[c]	455.0	–	397.3	–	4.21	–	455.1[6], 397.4[6]
TiO_2[d]	459.3	531.0	–	1.06	–	–	458.9[4],530.4[4]
Cr[c]	574.5	–	–	–	–	–	574.0[7]
Cr_2O_3[e]	577.0	530.9	–	–	–	1.54	576.8[8], 530.6[19]

a) Evaporated film

b) Air-oxidized evaporated film

c) Sputter deposited

d) Air-oxidized film of a)

e) Wet-H_2-fired sputter-deposited film, confirmed by x-ray diffraction.

f) Adjusted to Ag $3d_{5/2}$ = 368.2 eV, Au $4f_{7/2}$ = 84.0 eV or adventitious carbon at 285.0 eV, as required.

Table II XPS Peak Areas, TiN

	$2p_{3/2}$	O 1s	N 1s
Oxidized	19.20(TiN, 455.2eV)	11.15(TiO_2, 530.5eV)	4.56 (TiN, 397.4eV)
	2.35(TiO, 455.2eV)	4.99(TiO, 530.5eV)	3.43(N(a), 396.4eV)
	11.82(TiO_2, 458.7eV)	3.04(O^-/OH^-, Al_2O_3, 532.2e V)	
	6.17(Ti_2O_3, 457.1eV)		
Oxidized/			
Heated	28.14(TiN + TiO, 455.2eV)	15.03(TiO_2, 531.0eV)	7.81(TiN, 397.3eV)
	8.93(TiO_2, 458.9eV)	4.07(O^-/OH^-, Al_2O_3, 532.2eV)	1.16(N(a), 396.3eV)
	7.45(457.0eV)		

Table III XPS Peak Areas, Cr

	$2p_{3/2}$	O 1s
Oxidized	13.79 (Cr, 574.4eV) 38.45 (Cr_2O_3, 576.9eV)	24.69 (Cr_2O_3, 530.9eV)
Oxidized/ Heated	19.60 (Cr, 574.3eV) 32.81 (Cr_2O_3, 576.9eV)	22.54 (Cr_2O_3, 530.9eV)

7. Figure Captions

1. Total SEE yield, 140Å TiN on alumina: (– – –) after deposition, air exposure and bake at 550° in vacuo for 10hrs; (——) subsequently exposed to ambient atmosphere for 1 hour; (– · –) followed by electron bombardment of 3 x 10^{17} electrons/cm^2.

2. Ti 2p XPS core levels for conditions and legends corresponding to Figure 1; O(oxide), N(nitride).

3. 140Å Cr on alumina total SEE yield, same conditions and legends as Figure 1.

4. Cr 2p XPS core levels for conditions and legends corresponding to Figure 3; O(oxide), M(metal).

5. 140Å TiN/alumina, total SEE yield: (– – –), exposed to air, heated to 550°C for 2 hours; (——) heated at 550°C for 8 hours further; (– · –) re-exposed to air, heated to 250°C for 2 hours.

6. 140Å Cr on alumina, total SEE yield, same conditions and legends as Figure 5.

7. 140Å TiN on alumina, Ti 2p core levels, exposed to room air overnight: peaks 1 - TiN + TiO; peaks 2- Ti-suboxide; peaks 3- TiO_2. Total fit has χ^2=1.59. Small peak at ~450 eV is x-ray $\alpha_{3,4}$ satellite of peak 3.

8. 140Å TiN on alumina, exposed to air overnight. O 1s: peak 1-chemisorbed O and OH^-, peak 2-oxide, total fit χ^2=2.34. N 1s: peak 3-nitride, peak 4-adsorbed or interstitial N, total fit χ^2=1.45.

9. 140Å Ti on alumina, Ti 2p core levels, sample of Figures 7 and 8, following oxidation, heated at 550°C for 10 hours. Peak identification of Figure 7. Total fit χ^2=1.57.

10. 140Å TiN on alumina sample of Figure 9. Peak identification of Figure 8. Total fit χ^2 = 1.31 for O 1s, 1.72 for N 1s.

11. Reflection electron energy loss spectra for: (a) Ti, (b) TiO_2, (c) TiN, (d) oxidized TiN of Figure 7, (e) oxidized and heated TiN of Figure 9, (f) sum of (b) and (c) divided by 2. Features: 1 and 2 - first- and second-order bulk plasmon, 3 - surface plasmon, 4 - intraband transition. Primary electron energy was 300eV at 19.5° from normal incidence.

12. 140Å Cr on alumina, Cr 2p core levels, exposed to air overnight: peaks 1 - Cr metal; peaks 2 - Cr oxide. Total fit χ^2=3.85.

13. 140Å Cr on alumina, O 1s core level corresponding to Cr levels of Figures 12 and 14. Total fit χ^2=1.30 (oxidized) and 1.45 (oxidized/heated).

14. 140Å Cr on alumina, Cr 2p core levels, sample of Figure 12, following oxidation, heated at 550°C for 10 hours. Peak identification of Figure 12. Total fit $\chi^2 = 1.33$.

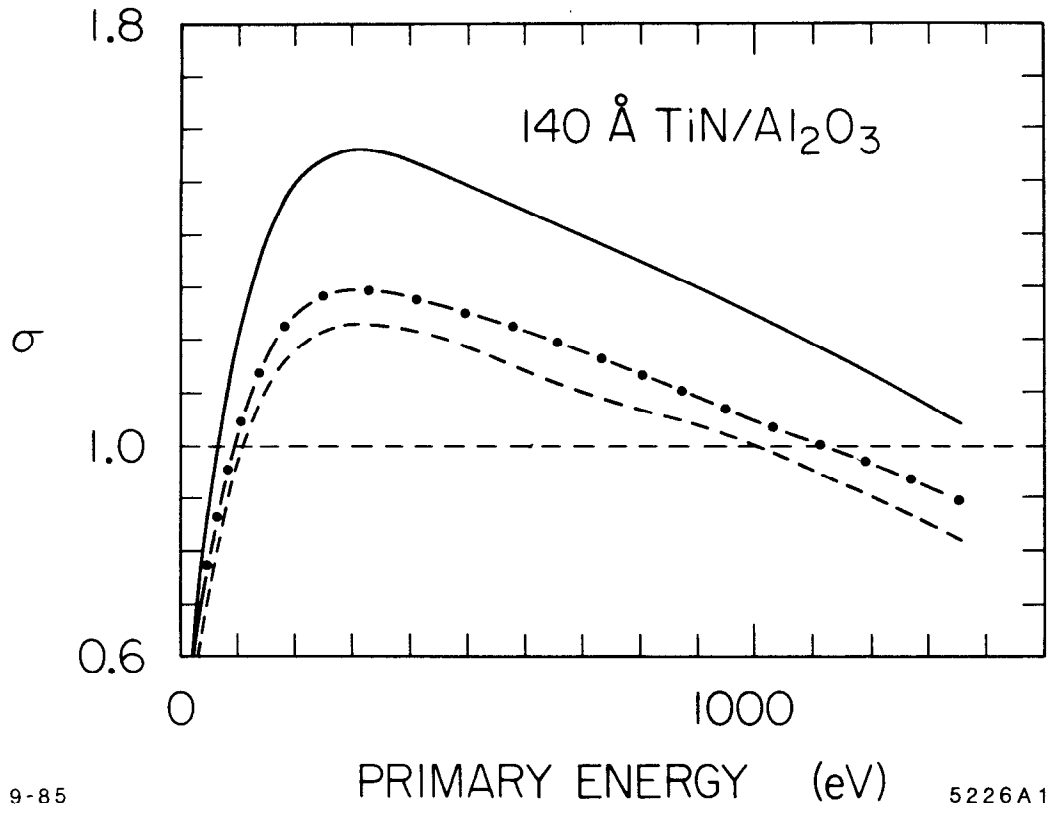

Fig. 1

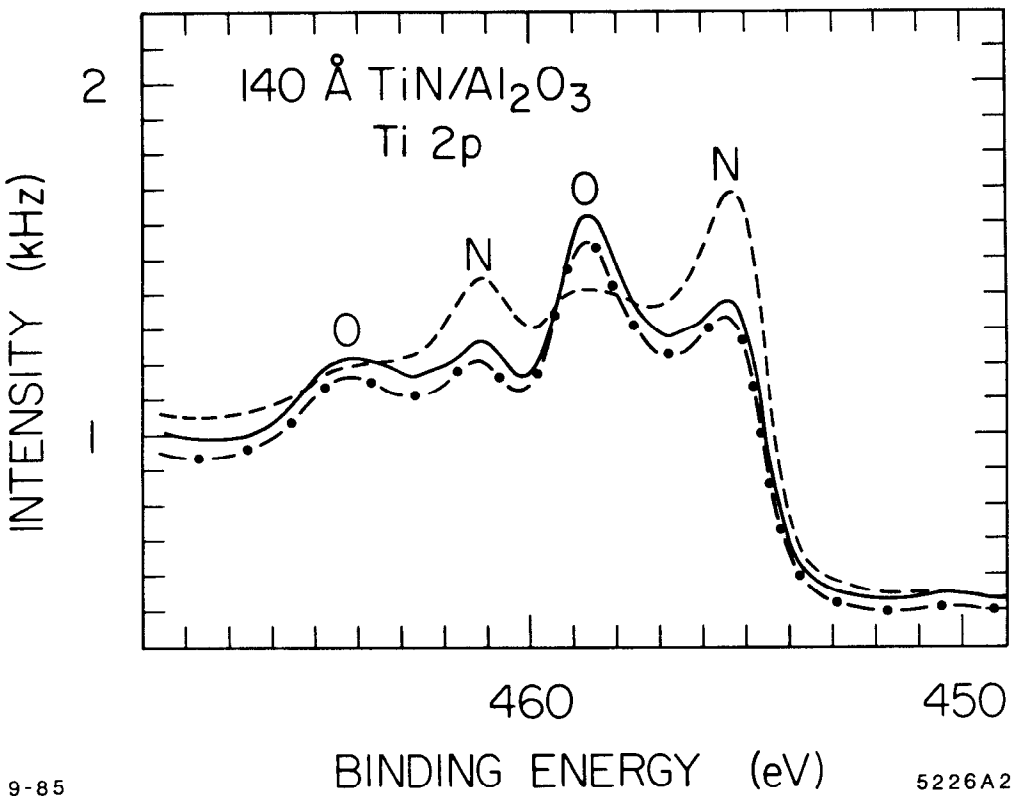
140 Å TiN/Al2O3
Ti 2p
O
N
O
N
2
1
INTENSITY (kHz)
460
450
BINDING ENERGY (eV)
9-85
5226A2

Fig. 2

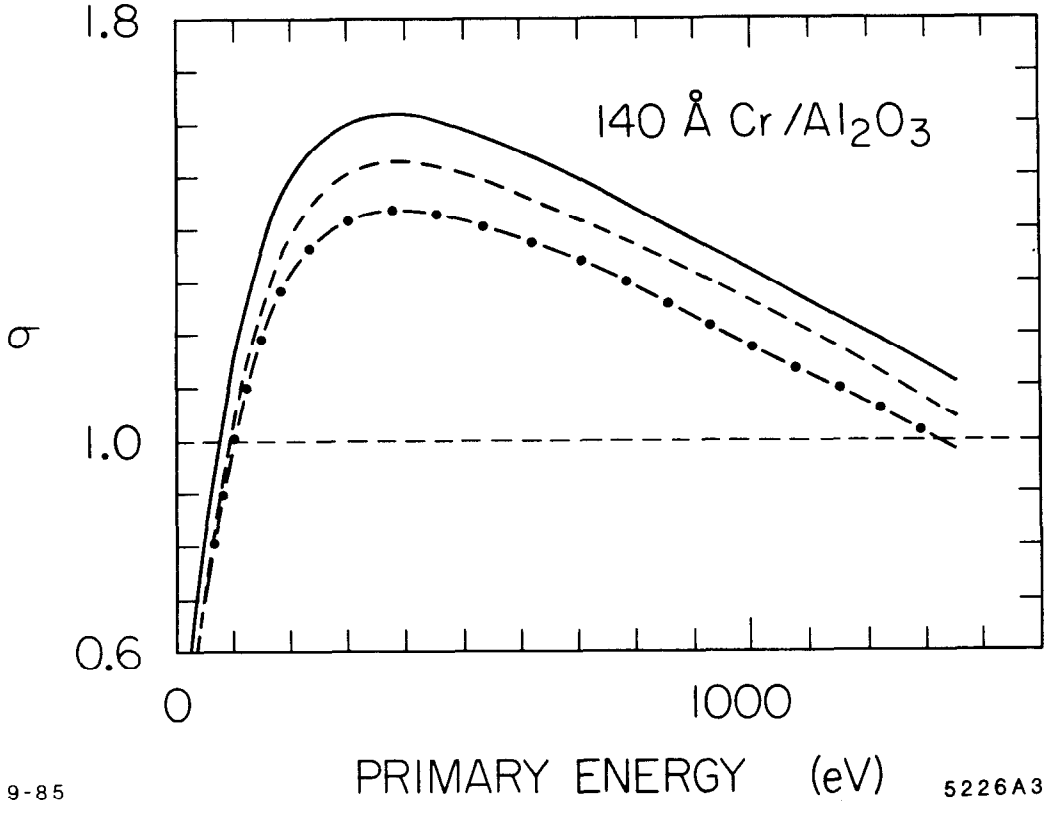

Fig. 3

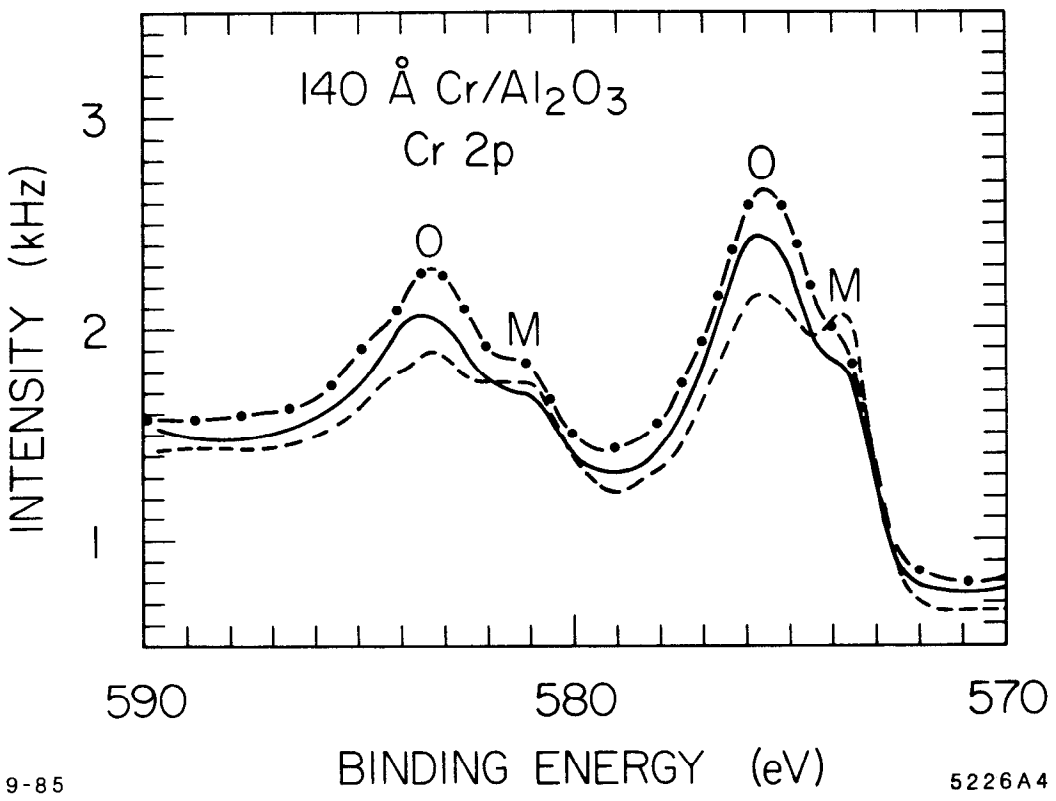
140 Å Cr/Al2O3
Cr 2p
O
M
O
M
INTENSITY (kHz)
3
2
1
590
580
570
BINDING ENERGY (eV)
9-85
5226A4

Fig. 4

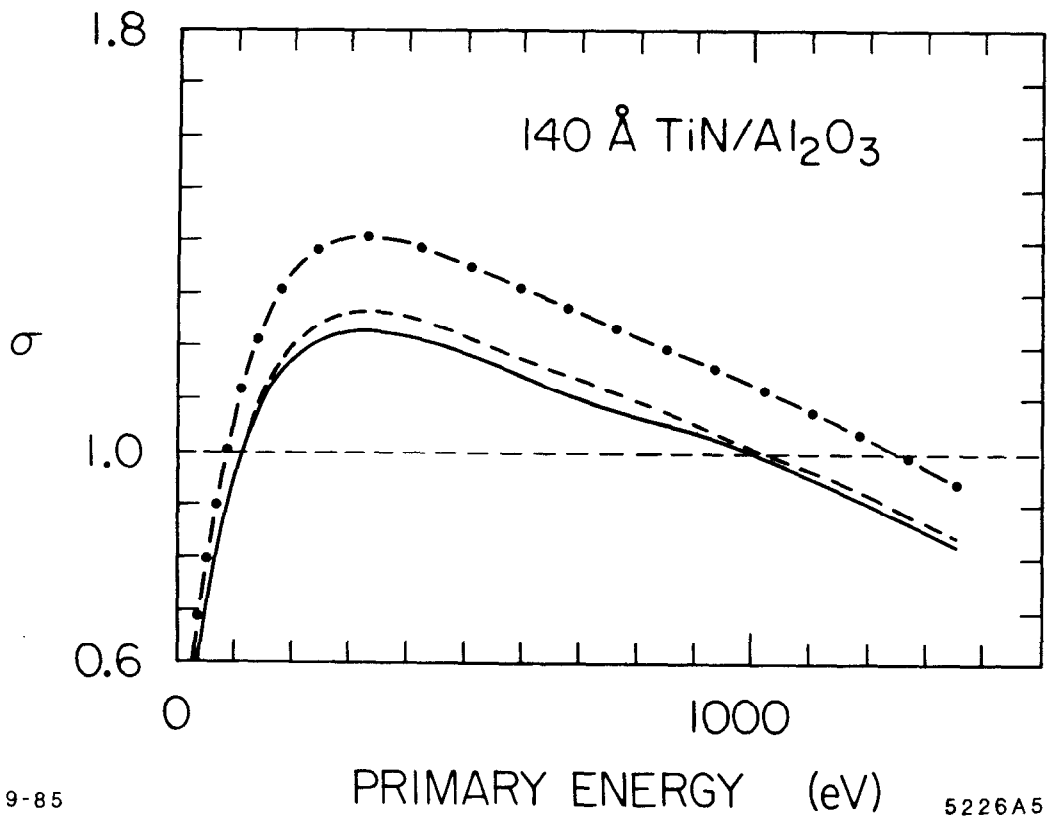

Fig. 5

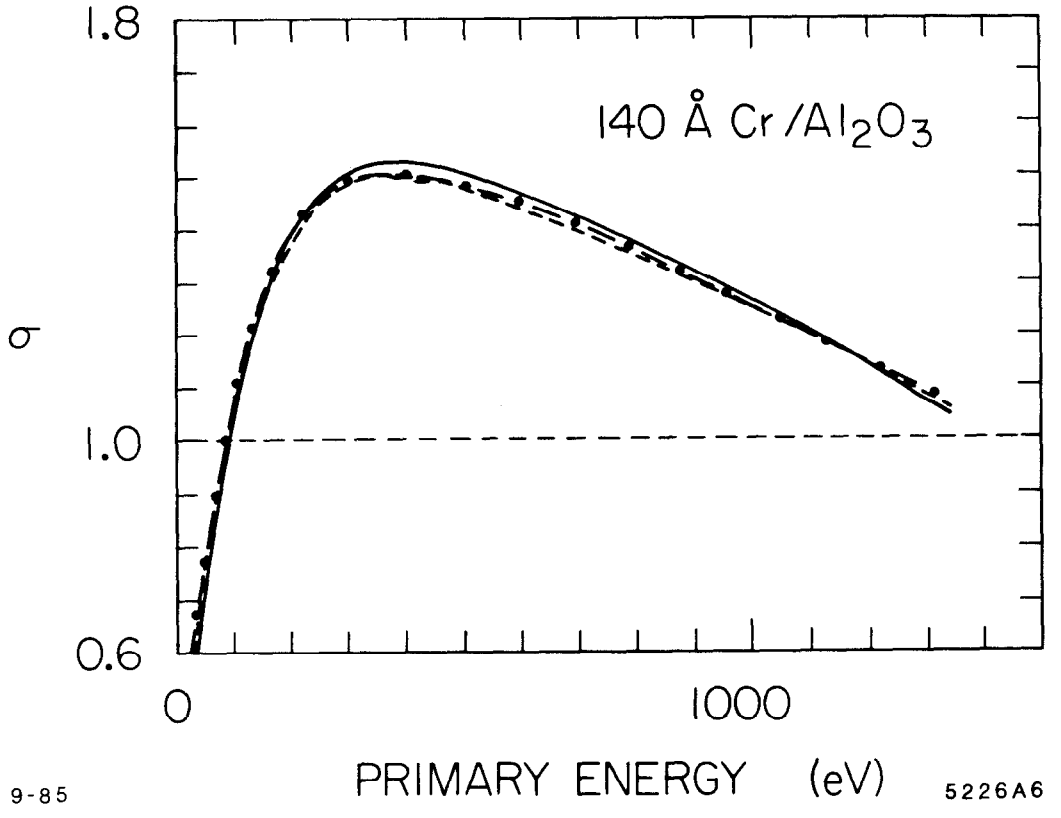

Fig. 6

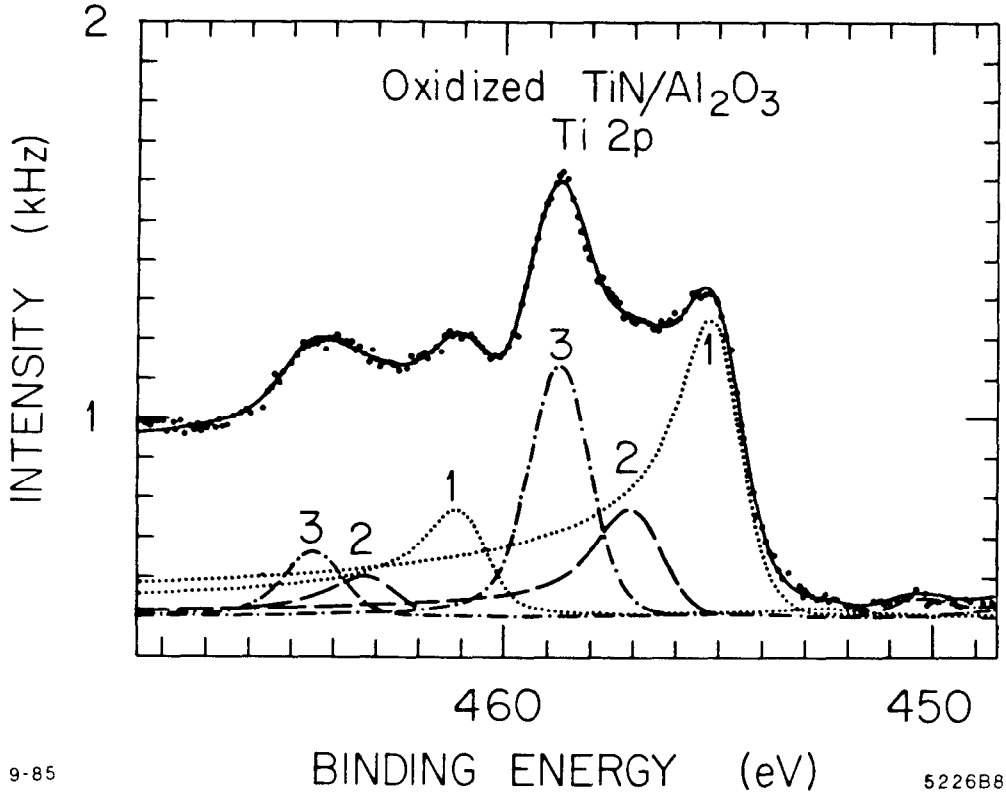
Oxidized TiN/Al2O3
Ti 2p
INTENSITY (kHz)
2
1
3
2
1
3
2
1
460
450
BINDING ENERGY (eV)
9-85
5226B8

Fig. 7

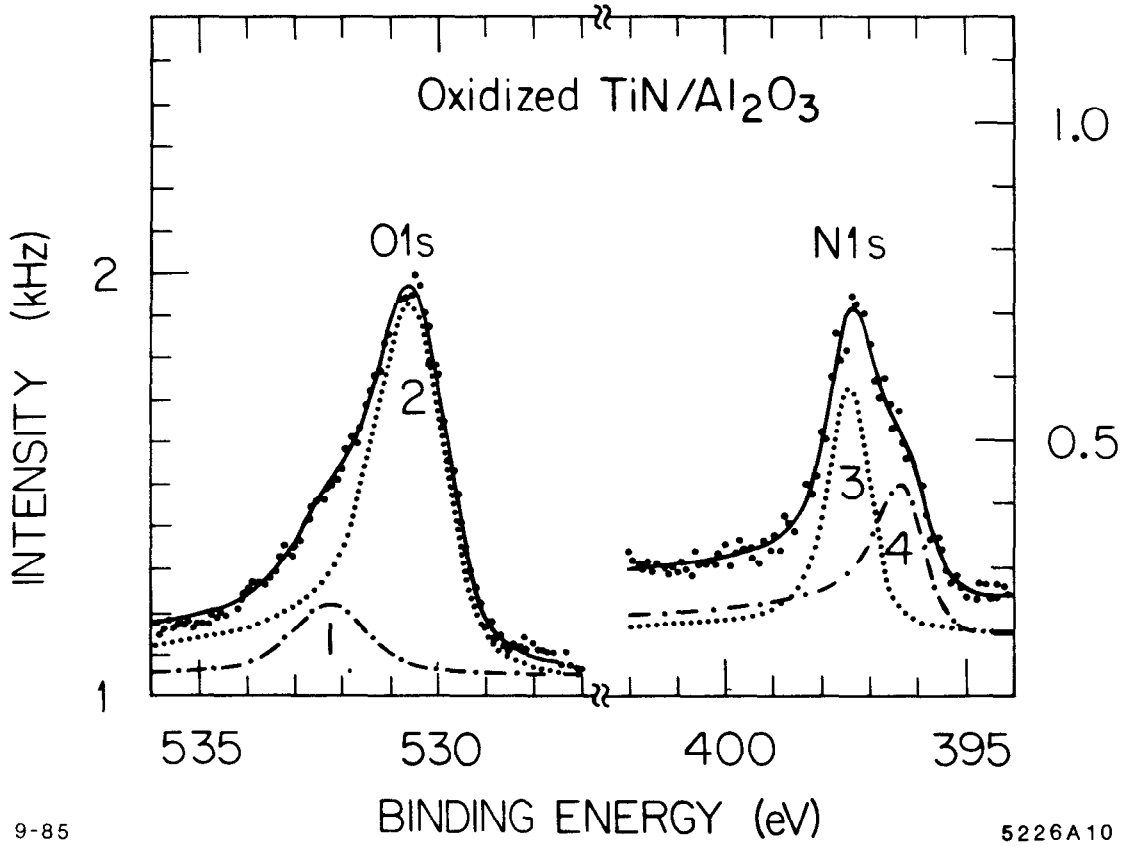
Oxidized TiN/Al2O3
O1s
N1s
INTENSITY (kHz)
2
1
1.0
0.5
535
530
400
395
BINDING ENERGY (eV)
1
2
3
4
9-85
5226A10

Fig. 8

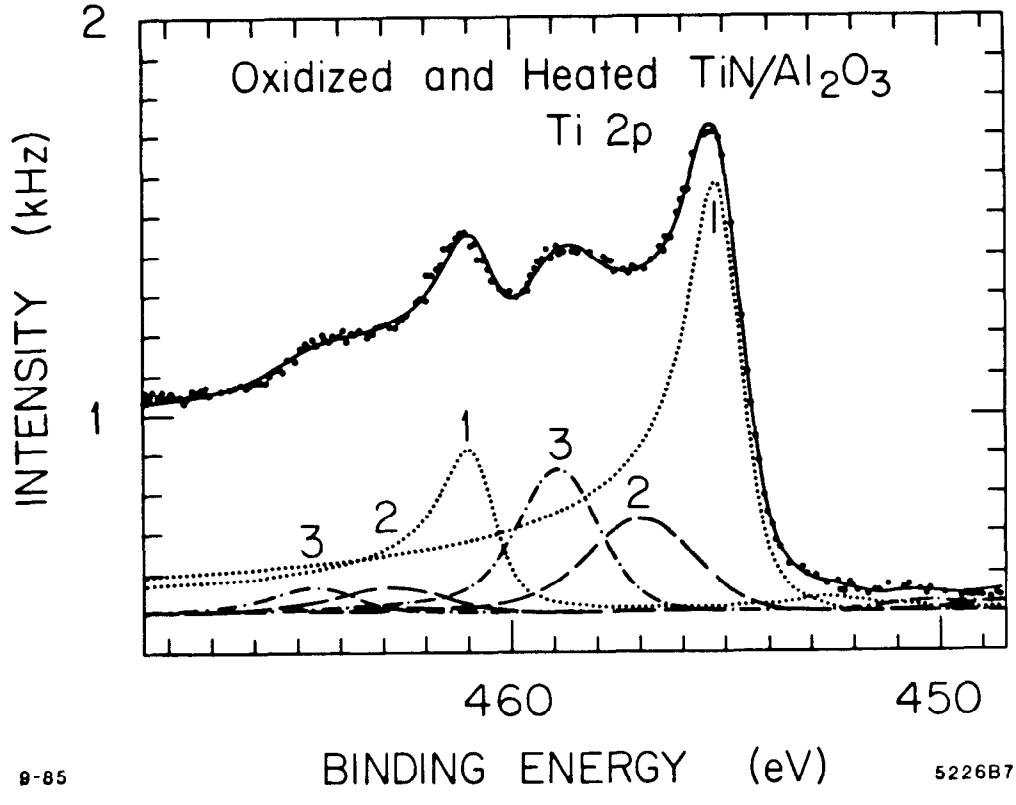
Oxidized and Heated TiN/Al2O3
Ti 2p
INTENSITY (kHz)
2
1
1
2
3
3
2
460
450
BINDING ENERGY (eV)
9-85
5226B7

Fig. 9

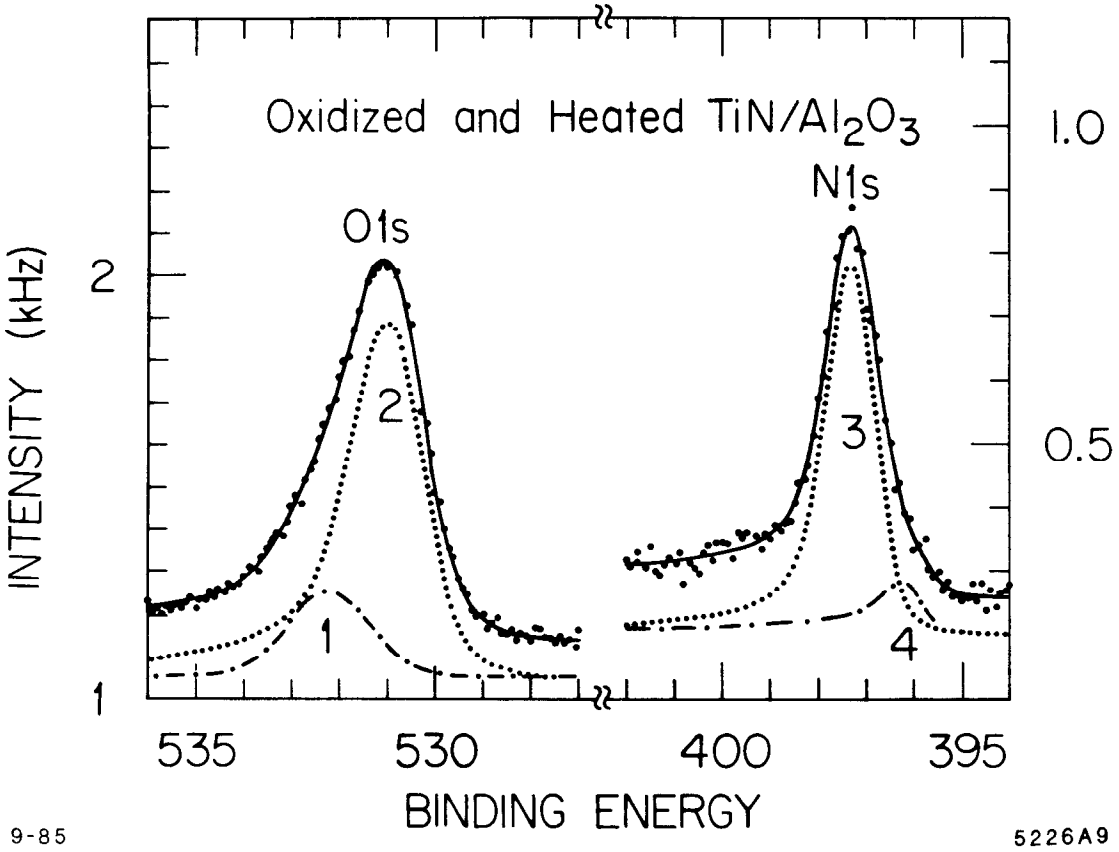
Oxidized and Heated TiN/Al2O3
O1s
N1s
1
2
3
4
INTENSITY (kHz)
2
1
1.0
0.5
535
530
400
395
BINDING ENERGY
9-85
5226A9

Fig. 10

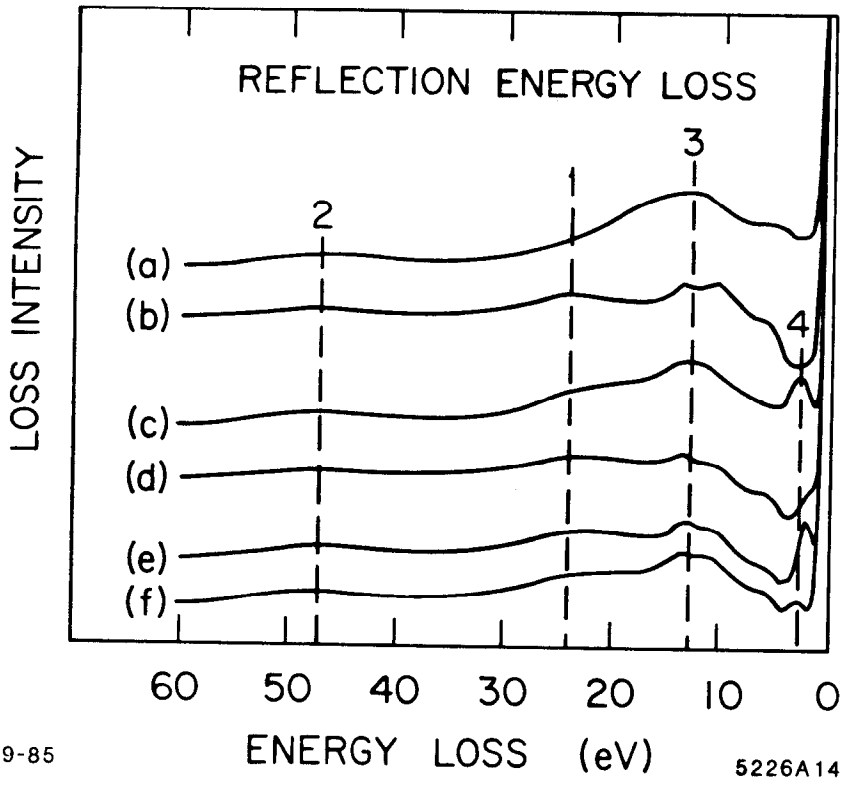
REFLECTION ENERGY LOSS
LOSS INTENSITY
2
3
4
(a)
(b)
(c)
(d)
(e)
(f)
60
50
40
30
20
10
0
ENERGY LOSS (eV)
9-85
5226A14

Fig. 11

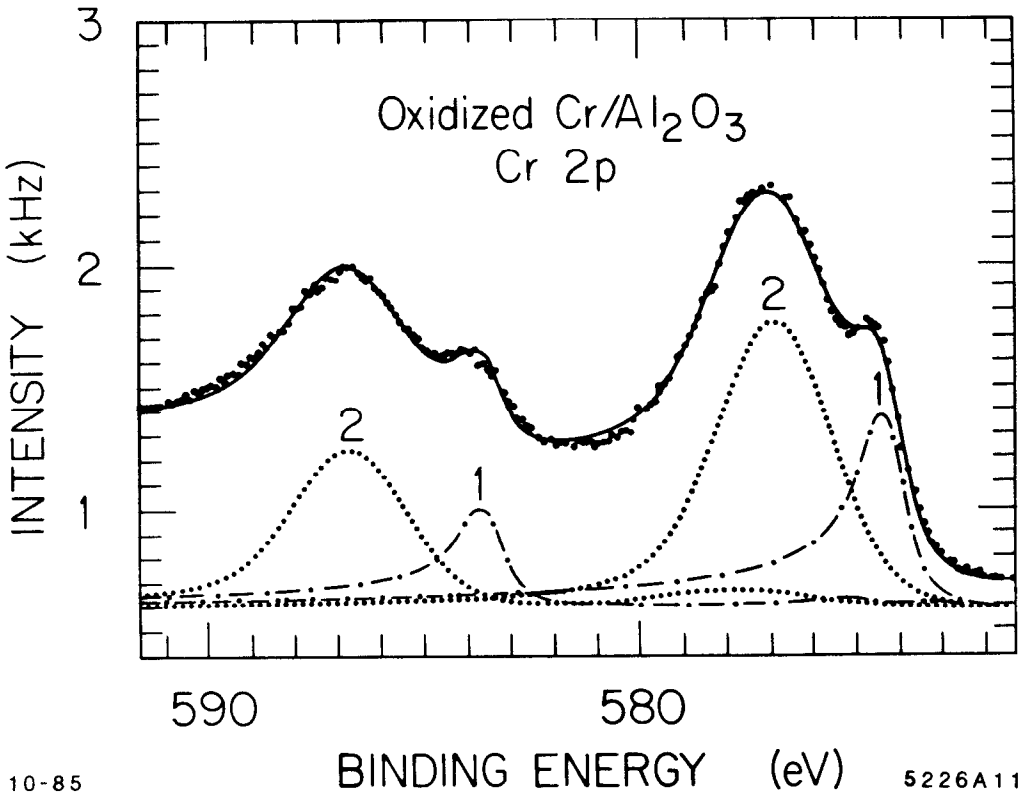
Oxidized Cr/Al2O3
Cr 2p
INTENSITY (kHz)
3
2
1
590
580
BINDING ENERGY (eV)
2
1
2
1
10-85
5226A11

Fig. 12

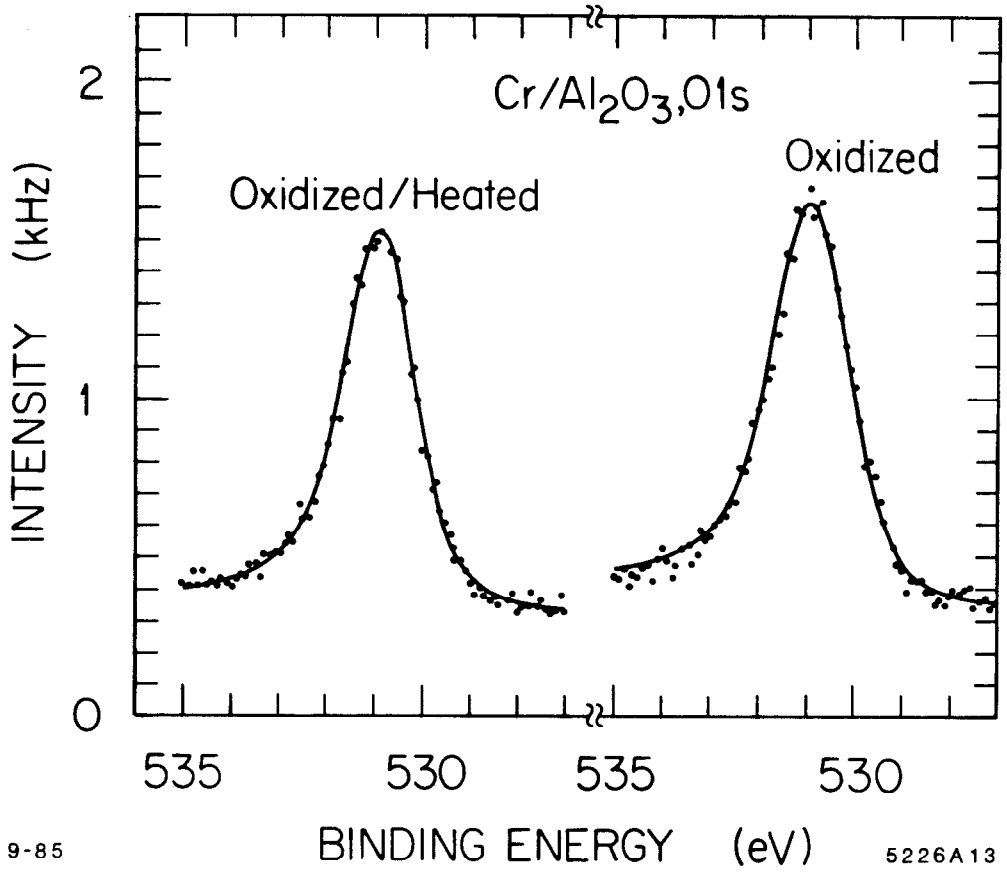
Cr/Al2O3,O1s
Oxidized/Heated
Oxidized
INTENSITY (kHz)
2
1
0
535
530
535
530
BINDING ENERGY (eV)
9-85
5226A13

Fig. 13

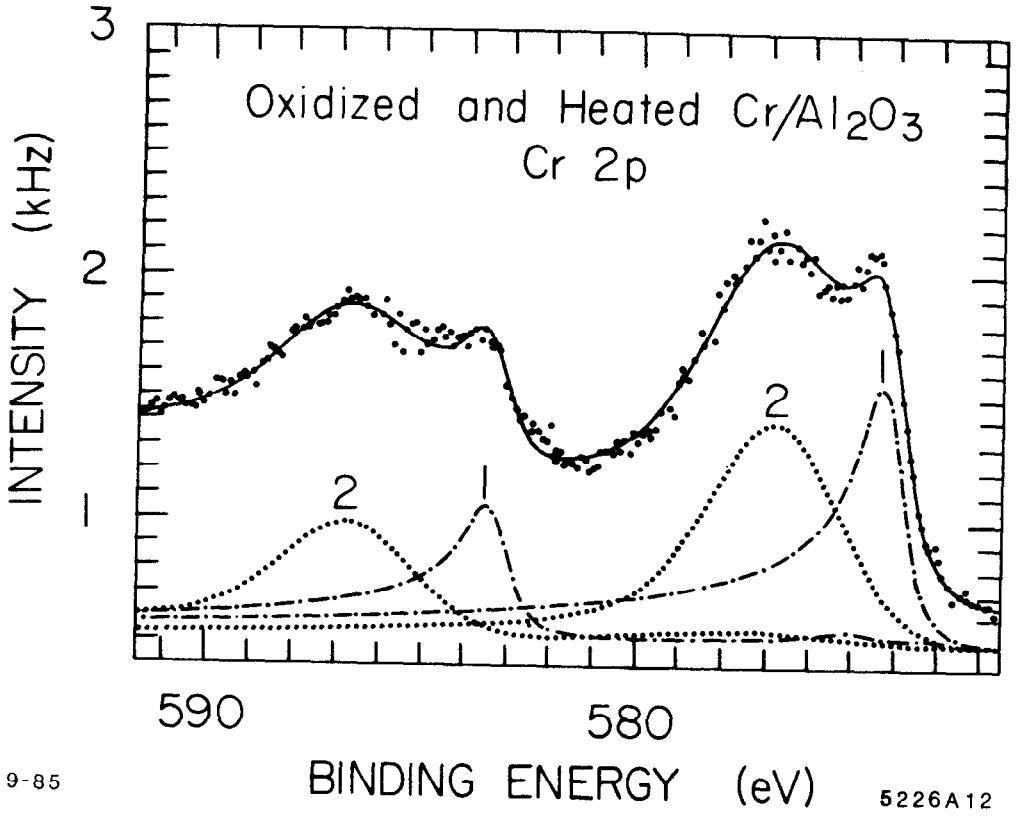
Oxidized and Heated Cr/Al2O3
Cr 2p
INTENSITY (kHz)
3
2
1
2
1
2
1
590
580
BINDING ENERGY (eV)
9-85
5226A12

Fig. 14